Supporting Information

Plasma-catalytic Direct Oxidation of Methane to Methanol over Cu-MOR: Revealing the Zeolite-confined Cu^{2+} Active Sites

Huan Lv,[#, a, b] Shengyan Meng,[#, a] Zhaolun Cui,[#, c] Shangkun Li,[d] Dongxing Li,[a] Xiaoxia Gao,[e] Hongchen Guo,[a] Annemie Bogaerts,[d] Yanhui Yi[a]*

[a] State Key Laboratory of Fine Chemicals, Frontier Science Center for Smart Materials, School of Chemical Engineering, Dalian University of Technology, Dalian 116024, P.R. China

[b] Baotou Electrical Industrial Vocational School, Baotou, 014000, P.R. China

[c] School of Electric Power Engineering, South China University of Technology, Guangzhou 510630, China

[d] Research group PLASMANT, Department of Chemistry, University of Antwerp, Universiteitsplein 1, BE-2610 Wilrijk-Antwerp, Belgium

[e] Instrumental Analysis Center, Dalian University of Technology, Dalian, 116024, P.R. China

* Corresponding author: Yanhui Yi

[#]: H.L., S.M. and Z.C. contributed equally to this paper

Email: yiyanhui@dlut.edu.cn

Table of Contents

1. Catalyst preparation

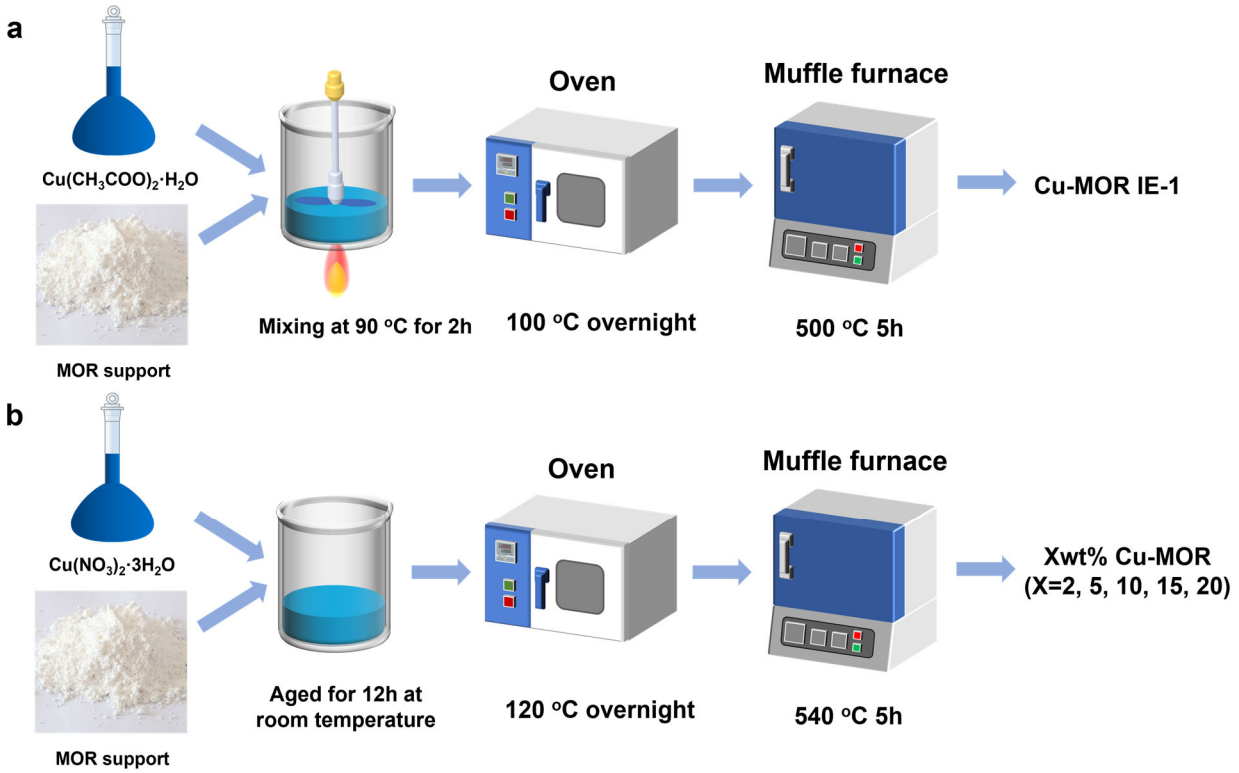

Scheme S1. Schematic diagram of Cu-MOR preparation procedure by (a) ion exchange method and (b) wetness impregnation method.

2. Experimental setup

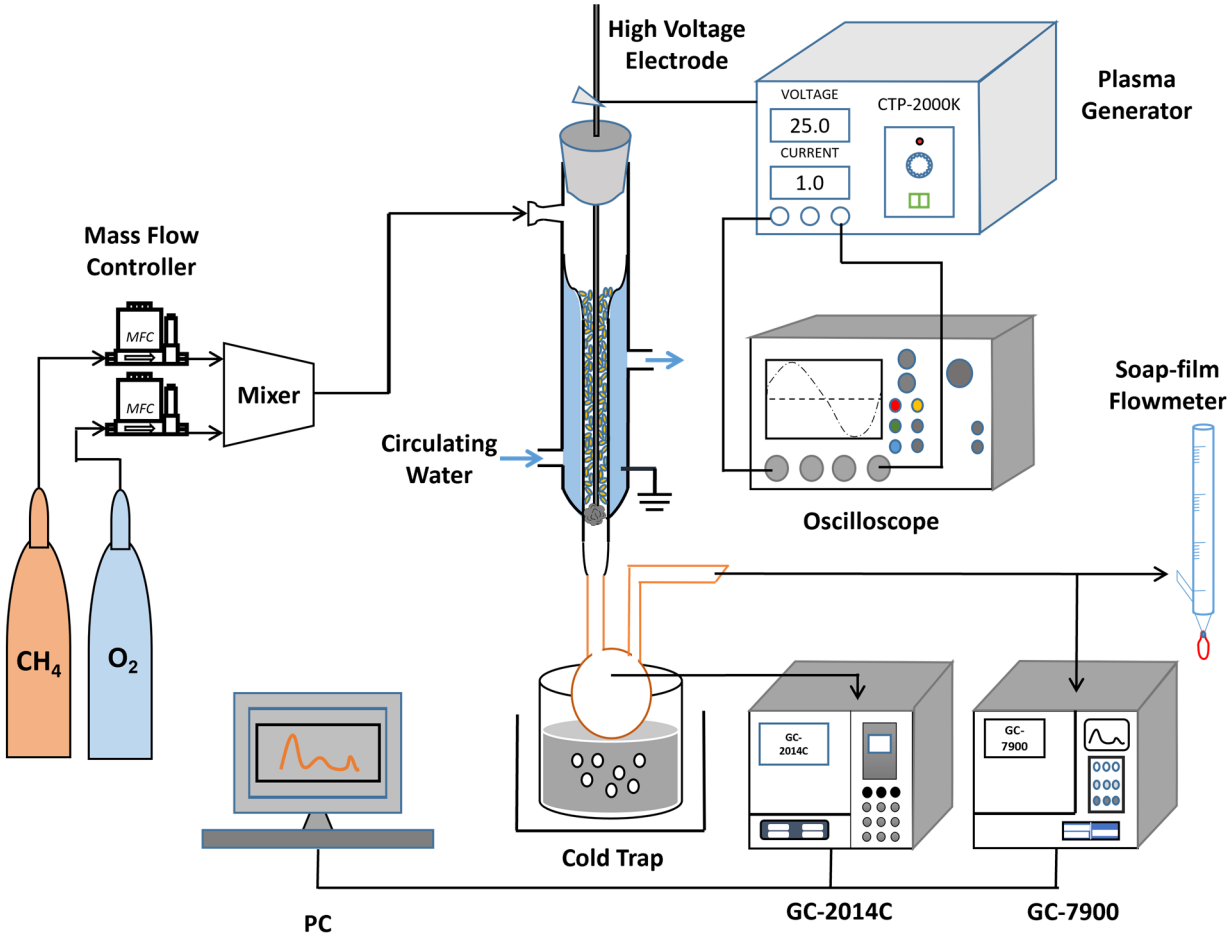

Scheme S2. Schematic diagram of the experimental setup.

3. Conversion and product analysis

Qualitative analysis

In NTP-promoted DOMTM, the feed gases (CH_4 and O_2) and gas phase products (CO, CO_2, C_2H_6) were analyzed on-line by GC-7900 gas chromatograph (TDX-01 column, alumina-filled column) equipped with thermal conductivity detector (TCD) and flame ionization detector (FID), and the results are shown in Figure S1a. Due to the low concentration of C_2H_6, quantitative studies were impractical with FID detection. The liquid-phase products were condensed in a collector using a cold trap (a mixture of isopropanol and liquid nitrogen) at temperatures not exceeding 120 °C. Offline analyses were later performed using gas chromatography GC-2014C, gas chromatography-mass spectrometry 5975C (GC-MS), and nuclear magnetic resonance spectrometry (^{1}H-NMR).

The GC results (Figure S1b) show the presence of methanol (CH_3OH), ethanol (C_2H_5OH), acetaldehyde (CH_3CHO), acetic acid (CH_3COOH), and propionaldehyde (C_3H_6O). The GC-MS results (Figure S1c) mainly show CH_3OH, formaldehyde (HCHO), and formic acid (HCOOH).^{1}H-NMR (Figure S1d) detected CH_3OH, HCOOH, and water (H_2O), in which dimethyl sulfoxide (DMSO) was an internal standard. Basically, these qualitative results confirm that the liquid products are H_2O, CH_3OH, HCHO, HCOOH, CH_3CH_2OH, CH_3CHO, CH_3COOH and C_3H_6O.

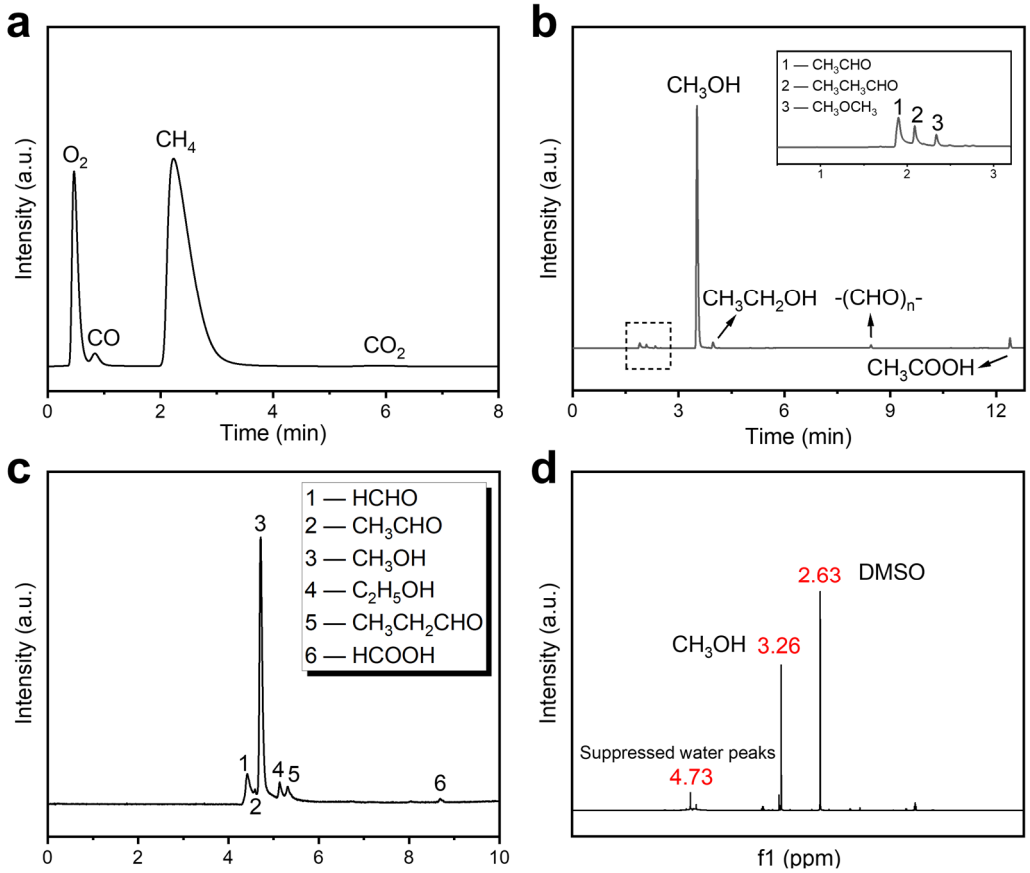

Figure S1. Results of qualitative analysis of the liquid products. (a) GC-7900 spectrum, illustrating the gas phase products of CO and CO_2; (b) GC-2014C spectrum, illustrating the presence of CH_3OH, CH_3CH_2OH, CH_3CHO, CH_3COOH and C_3H_6O; (c) GC-MS spectrum, illustrating the presence of CH_3OH, HCHO, HCOOH; (d) ^{1}H-NMR spectrum, illustrating the presence of CH_3OH, HCOOH and H_2O.

Quantitative analysis

After operating the CH_4/O_2 NTP for 2 h, the collected liquid sample was dripped with deionized water to 4 ml in the collector, then mixed uniformly and immediately transferred to the refrigerator for further analysis. For quantitative analysis, the concentrations of CH_3OH (methanol), C_2H_5OH (ethanol), CH_3CHO (acetaldehyde), CH_3COOH (acetic acid) and C_3H_6O (propionaldehyde) were determined by GC, while the concentration of HCHO (formaldehyde) was measured by GC-MS and the concentration of HCOOH (formic acid) was analyzed by ^{1}H-NMR with DMSO as internal standard in D_2O solvent.

The formulas of the standard calibrated concentration curves to calculate the product concentrations are listed in Table S1.

The CH_3OH productivity ($\mu mol \cdot g_{cat}^{-1} \cdot h^{-1}$) can be defined as follows, which can be well compared as a criterion for the performance of different catalysts on stoichiometric chemical looping using O_2. The reaction time was calculated only on duration of methane reaction, without considering the duration of CH_4 activation and CH_3OH extration in the chemical looping.

$$CH_3OH\ Produtivity = \frac{\text{moles of methanol produced (μmol/h)}}{\text{catalyst weight (g)}} \quad (1)$$

Table S1. Formulas of the standard concentration curves for each of the products.

Products	Analysis Method	Equation	Adj.R-Square
CH_4	GC	$Y=8.80358X\cdot10^{-8}+0.07257$	0.999
O_2	GC	$Y=8.23844X\cdot10^{-8}+0.01144$	0.999
CO	GC	$Y=7.40944X\cdot10^{-8}-9.04398\cdot10^{-4}$	0.999
CO_2	GC	$Y=7.06822X\cdot10^{-8}-0.01206$	0.999
CH_3OH	GC	$Y=92704.4X$	0.998
C_2H_5OH	GC	$Y=118790X$	0.998
CH_3CHO	GC	$Y=29678.5X$	0.998
CH_3COOH	GC	$Y=49613.1X$	0.999
CH_3CH_2CHO	GC	$Y=121251X$	0.998
CH_3COCH_3	GC	$Y=132411X$	0.998
HCHO	GC-MS	$Y = 5.9647X\cdot10^{-4} + 0.01673$	0.999
HCOOH	^{1}H-NMR	$Y = 0.4889X + 0.0354$	0.999

Y denotes the concentration of the sample, in mol/L; X denotes the peak area of the sample.

4. TGA and MS results under different discharge power

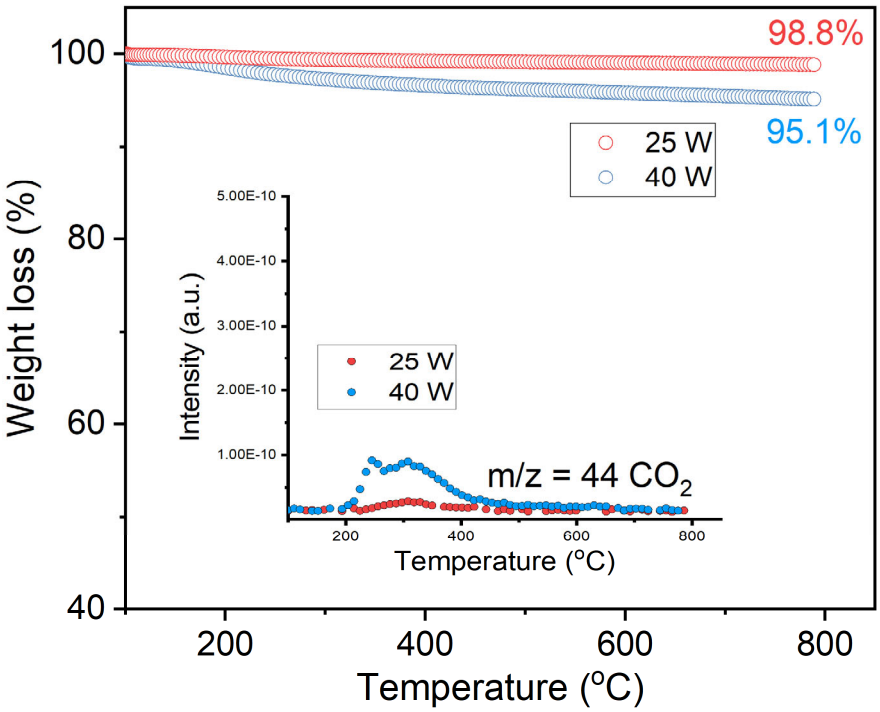

Figure S2. TGA and MS results under different discharge power of spent Cu-MOR IE-3.

5. The selectivity of other liquid products

Table S2. The selectivity of other liquid products in Figures 1a and 1b.

	CH_3CHO (Acetaldehyde)	CH_3CH_2CHO (Propionaldehyde)	CH_3COCH_3 (Acetone)	CH_3CH_2OH (Ethanol)	$CH_3CH_2CH_2OH$ (n-Propanol)	CH_3COOH (Acetic acid)
plasma only	3.98	0.36	0.06	0.99	0.03	2.26
MOR	1.79	0.02	0.1	0.65	0.01	2.86
IE-1	5.58	0.18	0.07	0.82	0.02	2.84
IE-2	2.54	0.19	0.19	0.98	0.01	2.73
IE-3	3.72	0.08	0.05	1	0.02	2.54
IE-4	3.85	0.08	0.05	1.2	0.02	3.15
IE-5	7.3	0.32	0.52	1.41	0.12	2.45
2%	2.85	0.92	0.27	1.35	0.03	4.67
5%	2.62	0.14	0.05	0.95	0.03	1.22
10%	2.52	0.23	0.04	0.68	0.04	1.79
15%	1.18	0.16	0.03	0.6	0.03	0.75
20%	1.2	0.03	0.01	0.45	0.06	0.36

6. *In-situ* FTIR reaction cell

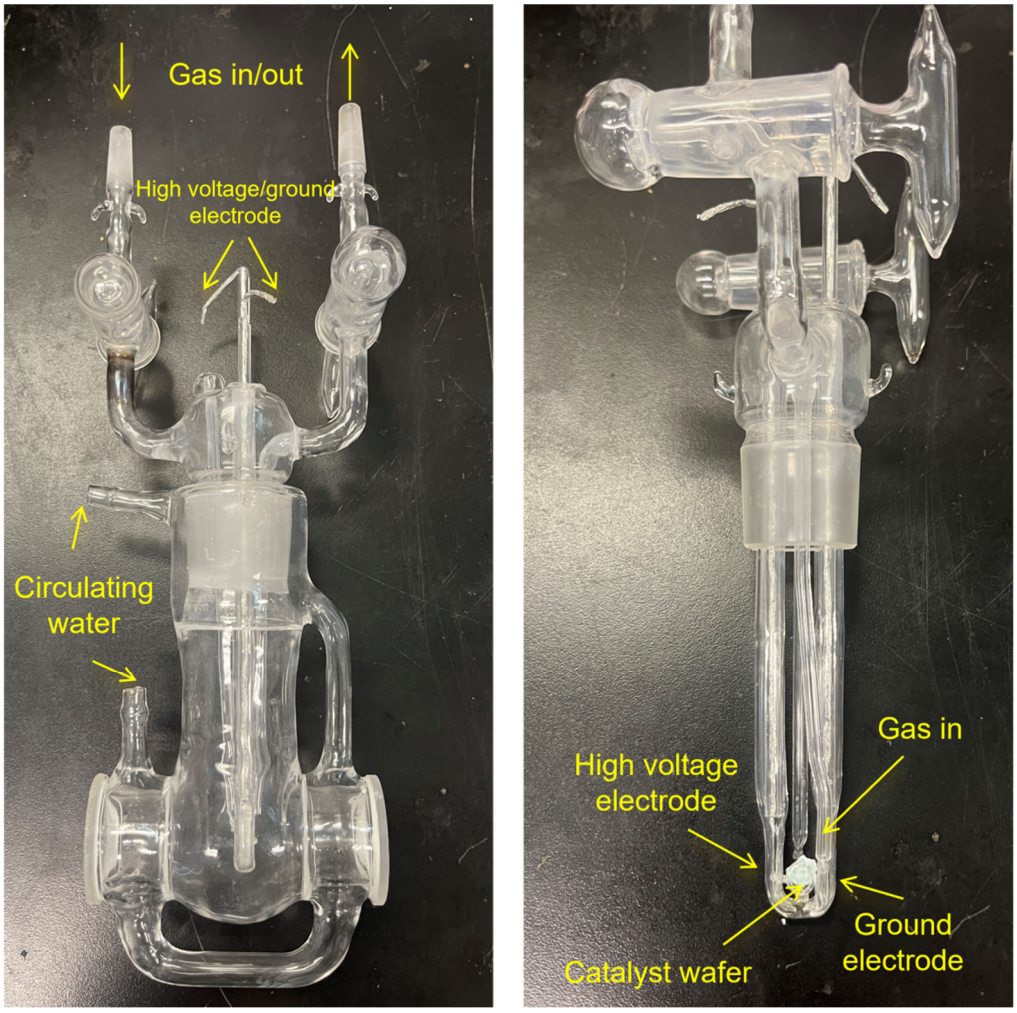

Figure S3. Schematic diagram of the *In-situ* FTIR reaction cell.

7. Energy consumption comparison

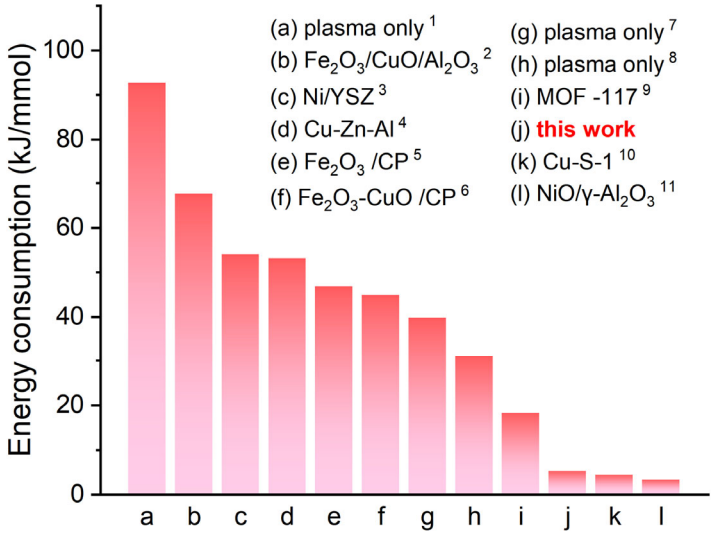

Figure S4. Comparison of this work with literature results of energy consumption.

Table S3. Comparison of this work with literature results of energy consumption.

Catalyst	Power (W)	Feed flowrate (ml/min)	CH_4 conv. (%)	CH_3OH sel. (%)	Energy con. (kJ/mmol)
plasma only [1]	118	150	6	19	92.7
$Fe_2O_3/CuO/Al_2O_3$ [2]	120	150	43	3.7	67.6
Ni/YSZ [3]	80	24	35.3	23.5	54.0
Cu-Zn-Al [4]	60	24	25.3	25	53.1
Fe_2O_3 /CP [5]	140	150	25.5	10.5	46.8
Fe_2O_3-CuO /CP [6]	140	150	25	11.2	44.8
plasma only [7]	200	750	3	30	39.8
plasma only [8]	20	85	5	20.4	31.0
MOF -117 [9]	7	24	18.4	11.7	18.2
Cu-S-1 [10]	15	160	5.8	50.6	4.3
NiO/γ-Al_2O_3 [11]	30	400	6.4	50	3.2
Cu-MOR (this work)	25	160	7.9	51	5.2

8. Catalyst characterization

N_2-physisorption and XRF

As shown in Table S4, the surface area and pore volume of the catalysts decreased with the increase of copper loading. It is more obvious especially for the Cu-based catalysts prepared by impregnation method, which may be due to the occupation of pore channels by copper oxide particles. The N_2 adsorption-desorption curves of Cu-MOR (Figure S5) reflect that all Cu-based catalysts are microporous materials. The Si/Al ratio of Cu-based catalysts fluctuated slightly with Cu loading, while the Cu/Al ratio increased significantly with ion exchanges times and Cu loading.

Table S4. Physical parameters of the supports and Cu catalysts

Catalysts	Si/Al ratio	Cu/Al ratio	Cu loading (%)	BET surface area (m^2/g)	Pore volume (cm^3/g)	Average pore size (nm)
MOR	16.74	0.00	0.00	484.4	0.18	1.89
Cu-MOR IE-1	16.37	0.19	2.16	469.8	0.17	1.94
Cu-MOR IE-2	17.09	0.27	2.89	459.5	0.16	1.93
Cu-MOR IE-3	16.99	0.31	3.39	453.1	0.16	1.93
Cu-MOR IE-4	17.10	0.34	3.68	457.0	0.16	1.93
Cu-MOR IE-5	17.02	0.39	4.16	454.7	0.16	1.93
2 wt.% Cu-MOR	16.93	0.23	2.48	495.2	0.18	1.91
5 wt.% Cu-MOR	17.09	0.44	4.70	464.6	0.17	1.92
10 wt.% Cu-MOR	19.12	1.04	10.23	434.5	0.16	1.96
15 wt.% Cu-MOR	17.01	1.63	14.94	410.2	0.15	1.96
20 wt.% Cu-MOR	16.89	2.48	20.76	365.9	0.13	2.00

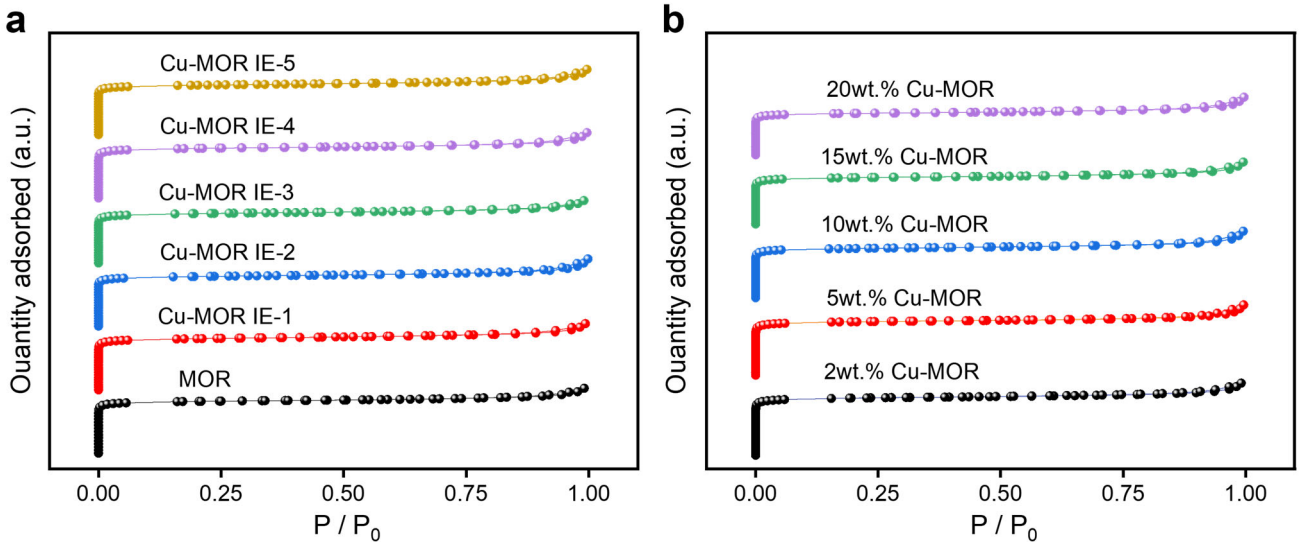

Figure S5. N_2 adsorption−desorption curves of Cu-MOR catalyst.

SEM

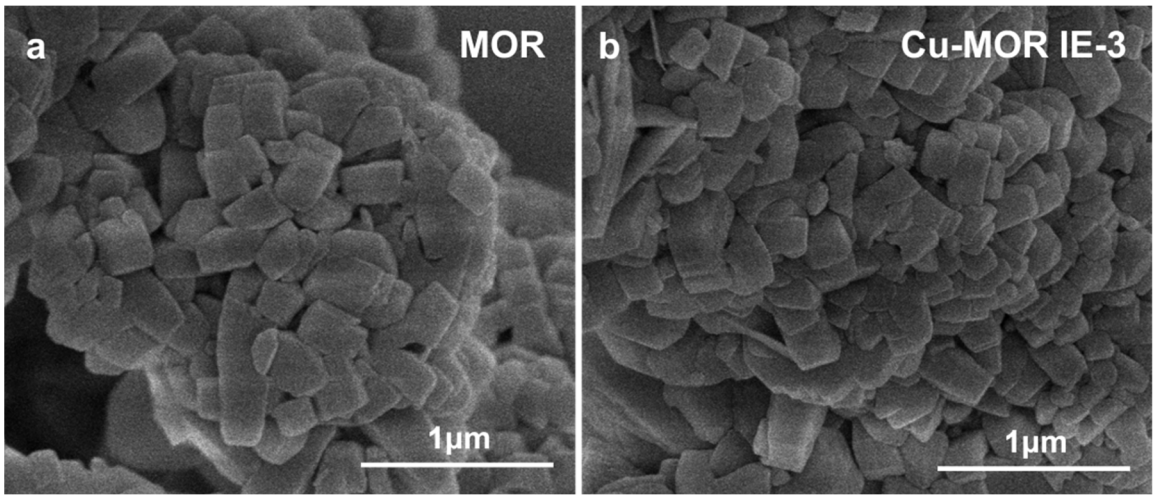

Figure S6. SEM results of (A) MOR and (B) Cu-MOR IE-3.

CO-DRIFTS

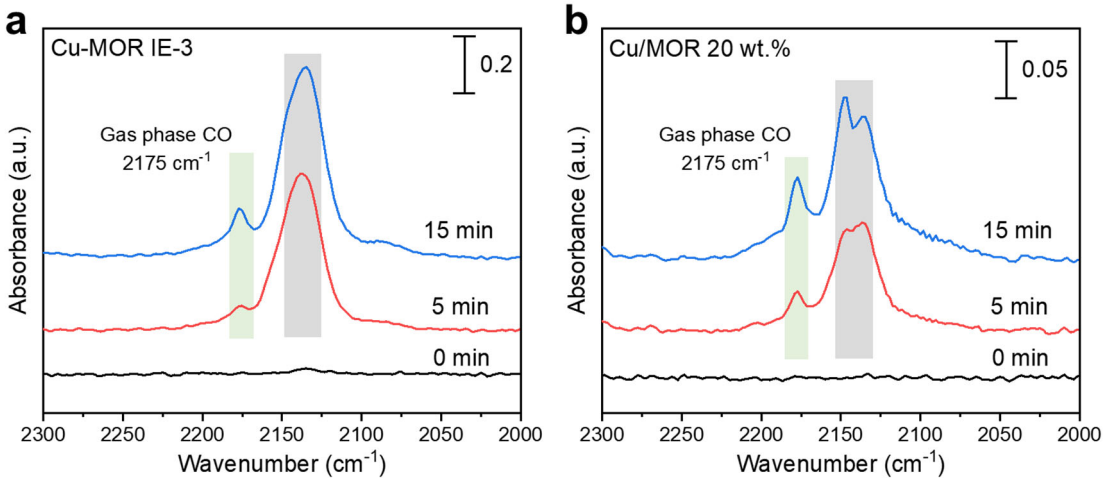

Figure S7. CO-DRIFTS results of (a) Cu-MOR IE-3 and (b) Cu/MOR 20 wt.%.

HRTEM

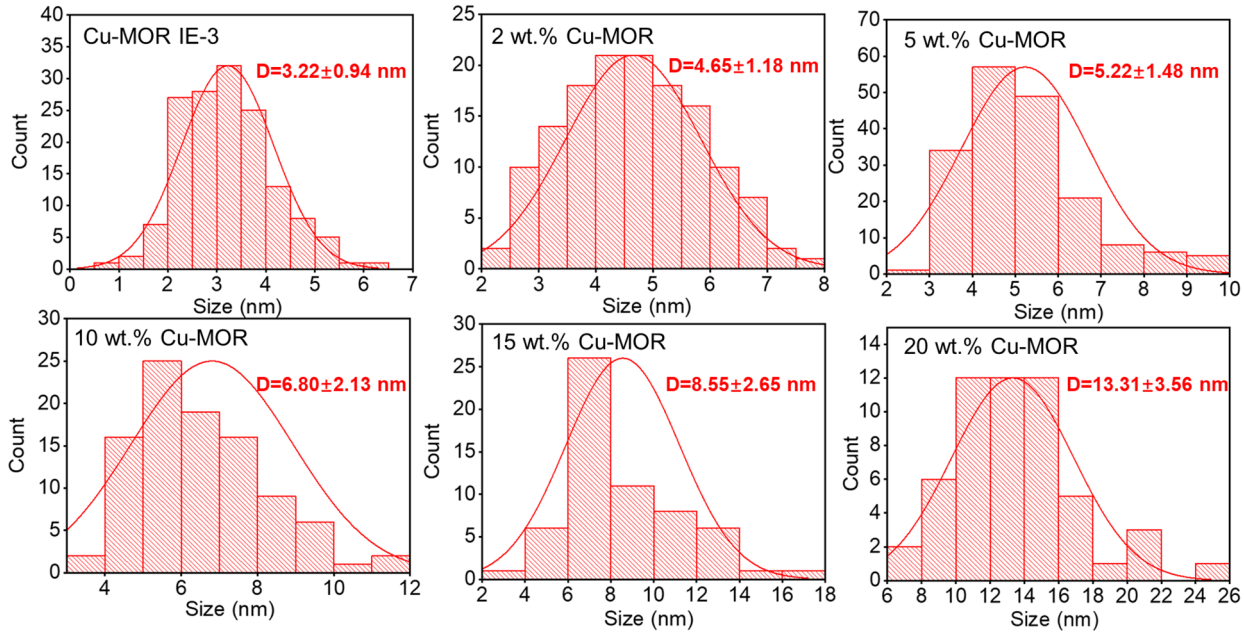

Figure S8. Particle size distribution of CuO particles in Cu-zeolite catalysts.

XPS spectra of Cu 2p$_{3/2}$

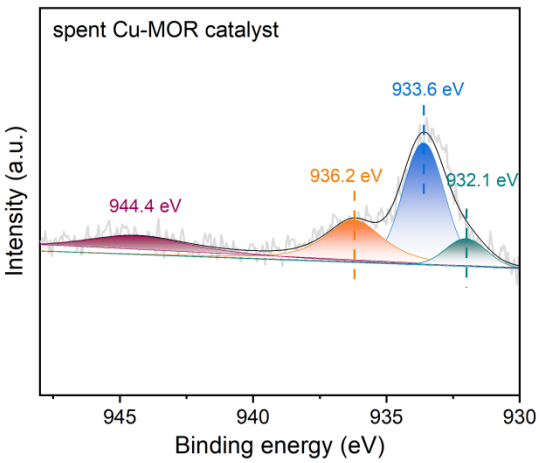

Figure S9. Cu 2p$_{3/2}$ spectra of the spent Cu-MOR IE-3 catalysts.

9. Temperature measurement for the plasma zone

Due to the presence of the plasma field, the reaction temperature in the plasma region/catalyst bed cannot be measured directly by thermocouples. In this paper, the temperature of the plasma region was measured using an infrared thermal imaging camera and the results are shown in Figure S10. It can be seen that the temperature of the inner wall of the reactor is around 28 °C, which is similar to the temperature of the circulating water grounding electrode (20 °C). The temperature in the center region of the catalyst bed is around 85 °C, which is mainly caused by two reasons. On the one hand, the exothermic nature of the CH_4 oxidation reaction raises the catalyst bed temperature; On the other hand, excitation of molecular vibrations caused by the high energy density electrons in the DBD plasma also causes gas heating by subsequent vibrational-translational relaxation.

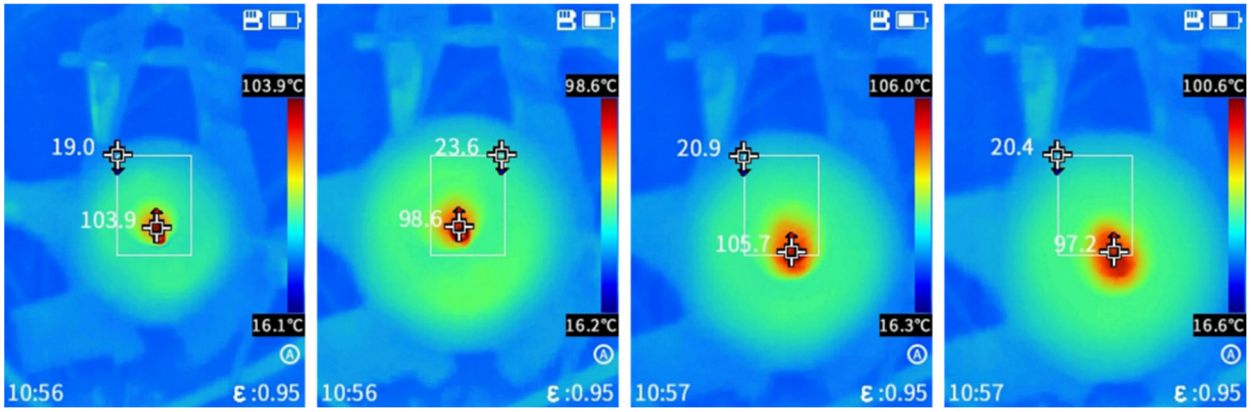

Figure S10. Temperature distribution of the DBD reactor during operation.

10. Calculation of the mean electron energy

The electron energy distribution function (EEDF) is calculated by Bolsig+. Its most important input, the reduced electric field (E/N), is calculated according to the method proposed by Mei et al.[12] Accordingly, we simplified the reactor tube (in Scheme S2) into four layers, i.e., the inner electrode, packing layer, gas layer and the outer dielectric layer. The thickness of each layer is determined by the reactor parameters and the packing degree of the catalysts. The mean electrical field (E-field) strength in the gas layer is calculated via the Gauss Law with the average sampling voltages and typical dielectric constants as inputs. In this study, the dielectric constants of MOR, Cu/MOR and the quartz tube are 2.4, 2.9 and 3.7, respectively. The discharge gap without packing is 3 mm. The packing fractions of MOR and Cu/MOR are 0.8. Subsequently, the E-field outputs are combined with the gas component to calculate the E/N values in non-packed, MOR-packed and Cu/MOR-packed systems. Gas compoments are selected from the experiments, i.e., CH_4 and O_2 at fractions of 80% and 20%, respectively. The discharge frequency is set at 9.2 kHz, with average voltage input by three times sampling. The cross-section data for possible reactions, including electron attachment, elastic collisions, electron impact excitation and ionization, are adopted from the Itikawa database in www.lxcat.net. All these data are used as inputs in Bolsig+, which calculates the mean electron energy against E/N and the EEDF.

REFERENCES

(1) D.W. Larkin, L.L. Lobban, R.G. Mallinson, The direct partial oxidation of methane to organic oxygenates using a dielectric barrier discharge reactor as a catalytic reactor analog, *Catal. Today* 71 (2001) 199-210.

(2) L. Chen, X. Zhang, L. Huang, L. Lei, Application of in-plasma catalysis and post-plasma catalysis for methane partial oxidation to methanol over a Fe_2O_3-CuO/γ-Al_2O_3 catalyst, *J. Nat. Gas Chem.* 19 (2010) 628-637.

(3) A. Indarto, H. Lee, J.W. Choi, H.K. Song, Partial oxidation of methane with yttria-stabilized zirconia catalyst in a dielectric barrier discharge, *Energy Sources Part A* 30 (2008) 1628-1636.

(4) A. Indarto, D.R. Yang, J. Palgunadi, J.-W. Choi, H. Lee, H.K. Song, Partial oxidation of methane with Cu-Zn-Al catalyst in a dielectric barrier discharge, *Chem. Eng. P. Int.* 47 (2008) 780-786.

(5) L. Chen, X.-W. Zhang, L. Huang, L.-C. Lei, Partial oxidation of methane with air for methanol production in a post-plasma catalytic system, *Chem. Eng. P. Int.*, 48 (2009) 1333-1340.

(6) L. Chen, X. Zhang, L. Huang, L. Lei, Post-Plasma Catalysis for Methane Partial Oxidation to Methanol: Role of the Copper-Promoted Iron Oxide Catalyst, *Chem. Eng. Technol.* 33 (2010) 2073-2081.

(7) L.M. Zhou, B. Xue, U. Kogelschatz, B. Eliasson, Partial oxidation of methane to methanol with oxygen or air in a nonequilibrium discharge plasma, *Plasma Chem. Plasma P.* 18 (1998) 375-393.

(8) D.L. Jurkovic, H. Puliyalil, A. Pohar, B. Likozar, Plasma-activated methane partial oxidation reaction to oxygenate platform chemicals over Fe, Mo, Pd and zeolite catalysts, *Int. J. Energy Res.* 43 (2019) 8085-8099.

(9) P. Chawdhury, Y. Wang, D. Ray, S. Mathieu, N. Wang, J. Harding, F. Bin, X. Tu, C. Subrahmanyam, A promising plasma-catalytic approach towards single-step methane conversion to oxygenates at room temperature, *Appl. Catal., B* 284 (2021) 119735.

(10) H. Lv, X. Liu, Y. Hao, Y. Yi, Coupling of Dielectric Barrier Discharge and Cu-S-1 Catalyst for Direct Oxidation of Methane to Methanol, *Plasma Chem. Plasma P.* 43 (2023) 1963-1978.

(11) Y. Yi, S. Li, Z. Cui, Y. Hao, Y. Zhang, L. Wang, P. Liu, X. Tu, X. Xu, H. Guo, A. Bogaerts, Selective oxidation of CH_4 to CH_3OH through plasma catalysis: Insights from catalyst characterization and chemical kinetics modelling, *Appl. Catal., B* 296 (2021) 120384.

(12) D. Mei, X. Zhu, Y.-L. He, J.D. Yan, X. Tu, Plasma-assisted conversion of CO_2 in a dielectric barrier discharge reactor: understanding the effect of packing materials, *Plasma Sources Sci. T.* 24 (2015) 015011.